PCCP

Accepted Manuscript

ROYAL SOCIETY OF CHEMISTRY

www.rsc.org/pccp

A linear diffusion model for ion current across blocking grain boundaries in oxygen-ion and proton conductors

Seong K. Kim[1], Sergey Khodorov[2], Igor Lubomirsky[2]* and Sangtae Kim[1]*

[1]Department of Chemical Engineering and Materials Science, University of California, Davis, CA 95616, USA
[2]Department of Materials Science, Weizmann Institute of Science, Rehovot, 76100, Israel

*Correspondence to: chmkim@ucdavis.edu; Igor.Lubomirsky@weizmann.ac.il;

Abstract

We demonstrate the applicability of the linear diffusion model recently proposed for the current-voltage, I_{gb}-U_{gb} , characteristics of blocking grain boundaries in solid electrolytes to various oxygen-ion and proton conductors: The model precisely reproduces the I_{gb}-U_{gb} characteristics of La-, Sm-, Gd-, and Y-doped ceria as well as Y-doped barium zirconate to provide accurate explanations to the "power law" behavior of the I_{gb}-U_{gb} relationships, i.e. $I_{gb} \propto U_{gb}^{n}$, experimentally observed. The model also predicts that the grain-boundary potential, Ψ_{gb}, in doped ceria weakly depends on temperature, if the trapped charge remains constant, and that the value of the Ψ_{gb} can be determined from the value of the power *n*. Furthermore, the model provides a plausible explanation for the increase in the Ψ_{gb} with temperature observed for the proton conductor in which the concentration of the charge carrier decreases with temperature. Hence, it is evident that the linear diffusion model is robust and applicable to grain boundaries in a large variety of practically important solid electrolytes.

Keywords: ionic conductivity, grain boundaries, *I-V* relationships; diffusion, impedance spectroscopy, doped ceria, barium zirconate

1 Introduction

Polycrystalline ceramics with high ionic conductivity are of great interest because of their potential use for advanced electrochemical energy devices (e.g. low-temperature solid-state fuel cells and all-solid-state batteries) as electrolytes[1,2]. However ion current in numerous solid electrolytes is often limited by grain boundaries [3-24] and it is becoming more important than ever

to have precise mechanistic knowledge of the current across the highly resistive grain boundaries. Recently we proposed a simple linear diffusion model that allows for accurate interpretation of the current-voltage characteristic of the grain boundary (hereafter I_{gb}-U_{gb} characteristics) in a popular oxygen-ion conductor, Y-doped CeO_2 (YDC).[25] The blocking nature of the grain boundaries in doped ceria is attributed to a potential barrier formed at the grain boundary.[3-5,10,14,20,21] Under the assumptions made, we demonstrated that[25]; (1) our model accurately reproduced the "power law" behavior of the I_{gb}-U_{gb} relationship (i.e. $I_{gb} \propto U_{gb}^{n}$) experimentally observed, which may not be explained by a conventional model based on thermionic emission (TE) theory.[26-28] Namely the TE model was originally developed and employed to describe an electronic current across a potential barrier at a metal-semiconductor contact, e.g. a Schottky diode. This model predicts that the I_{gb} initially increases linearly with U_{gb} to show the ohmic behavior and quickly deviates from it as the U_{gb} further increases to eventually follow exponential behavior, i.e. $I \propto e^{U_{gb}}$, at the U_{gb} higher than the thermal voltage, $V_{th} = k_B T / q$ (k_B, T, and q denote the Boltzmann constant, absolute temperature, and an elementary charge, respectively. See Section 3.3 below for more details). (2) Furthermore our model correctly predicts that the product $n \cdot T$ (with n being the power) is nearly constant in a sufficiently narrow range of temperature (see Section 2.2 for further discussion), and proportional to the grain-boundary potential, Ψ_{gb}, as long as the charge at the grain-boundary core remains unchanged, i.e. $n \cdot T \approx (0.41 q / k_B)\Psi_{gb}$. (3) Most importantly, this relationship allows for direct determination of the Ψ_{gb} from the power value n, and promises considerable simplification in the analysis of the I_{gb}-U_{gb} characteristics of ionic conductors with respect to the TE model currently in use.

In the present study, we demonstrate the robustness of our model. Firstly, to further verify our model, we measured the I_{gb}-U_{gb} characteristics of various CeO_2 doped with rare-earth cations (La^{3+}, Sm^{3+}, Gd^{3+}) and provide accurate explanations for their temperature dependence using our model. As will be shown below the I_{gb}-U_{gb} relationships of all those oxygen-ion conductors precisely obey the power law as our model predicted and Ψ_{gb} estimated from the power value n largely remains constant in the temperature range of interest. Secondly, we consider the grain boundaries in a proton conductor, Y-doped $BaZrO_3$. While the concentration

of mobile ions in the bulk, C_i^+, of the oxygen-ion conductors is independent of temperature, that of the proton conductor reduces with temperature due to water loss. This fact leads to, in contrast to the former, an increase in Ψ_{gb} with temperature in the latter. Our model also provides a theoretical explanation of such temperature dependence of the Ψ_{gb} in proton conductors. The values of the Ψ_{gb} in all the materials investigated in this study and their temperature dependence determined from our model will be compared with those from the conventional method based on the brick-layer model (BLM)[29].

2 Theoretical Considerations

2.1 The linear diffusion equation for the current across the grain boundary

The linear diffusion model for a material containing a single type of mobile ion is based on the three fundamental assumptions (for the sake of consistency, we retain all the notations defined in ref. [25]):

a) A grain boundary in an ionic conductor is considered a region with permanently trapped charge (irrespective of its origin) distributed over a region with a width of d_{real} and a charge density of N_{gb} (x). For simplicity's sake, we used a Gaussian distribution for the trapped charge.

b) A grain boundary does not constitute a physical barrier for diffusion and the diffusivity of the charge carrier remains constant throughout the material. The Nernst-Einstein relation for the electrical mobility is held true.

c) The mobile ions follow Boltzmann distribution.

The diffusion equation which concerns such a situation is well established[30-34] and is given in great details in ref.[35] Written with respect to electric field, $\phi(x)$, it reads:

$$\phi''(x)+[\phi'(x)+n_{gb}^{+}(x)-1]\cdot\phi(x)+\frac{\partial n_{gb}^{+}(x)}{\partial x}-j=0 \quad \text{for } x\in[0,\ L],\ L \text{ is the grain size} \tag{1}$$

For direct comparison between different cases, Eq (1) was converted into a dimensionless form using a set of standard normalization constants given in ref.[25] and reproduced here in Table 1. Accordingly, length is in the unit of Debye length, L_D; potential, φ, in the unit of the V_{th}; and the local concentration, $n_i^+(x)$, is measured in the unit of C_i^+, which is the concentration of mobile species in the bulk where the charge neutrality is held true. Electric field is measured in units of $-V_{th}/L_D$. In this normalization, the distribution of trapped charges is given as:

(2) $$n_{gb}^{+}(x) = N_{gb}^{+}(x) / C_i^{+} = \frac{a}{d \cdot \sqrt{\pi}} \exp\left(-\frac{x^2}{d^2}\right)$$

and a grain boundary is characterized by two important normalized parameters: the width, $d = d_{real} / L_D$, and the total charge of the grain boundary, a,

(3) $$a = Q_{gb} / (C_i^{+} \cdot L_D)$$

is normalized with respect to the real charge density Q_{gb}. The boundary conditions $\phi(0) = \phi(L)$ and $\phi'(0) = \phi'(L)$ automatically impose charge neutrality [25] by adjusting the total of the mobile species $\int_0^L n_i(x)\,dx$ to be exactly equal to the concentration of the immobile charges.

The solution of Eq. (1) results in a static I_{gb}-U_{gb} relationship that has three distinctive regions (see e.g. Figure 1 in this work or Fig. 1 in ref. [25] for the result of the numerical solutions)

i) As long as the U_{gb} is small, i.e. $U_{gb} < \sim 2\ V_{th}$, the grain boundary serves as a constant resistor.

ii) If the U_{gb} increases above $\sim 5\ V_{th} < U_{gb} < \sim 80\ V_{th}$, the I_{gb}-U_{gb} relationship can be approximated as a power law $I_{gb} \propto U_{gb}^{n}$, providing the explanation to the "power law" behavior of the I_{gb}-U_{gb} relationships previously reported for several ionic conductors. The power value of n decreases with decreasing grain boundary potential φ_{gb} ($\Psi_{gb} = \varphi_{gb} \cdot V_{th}$ in real notations) and $n \approx 0.41 \cdot \varphi_{gb}$. In a sufficiently narrow range of temperatures, the relation leads to $n \cdot T \approx const$ (or $n \cdot V_{th} \approx const$), which can serve as a criterion for verification of the applicability of the model.

iii) If U_{gb} increases above ~ 80 V_{th}, the depletion region starts to disappear and vanishes completely for U_{gb} > 300 V_{th} and the I_{gb}-U_{gb} relationship becomes linear again. However, such behavior may hardly be observable experimentally because application of 100 V_{th} to a single grain boundary requires application of many kV to a ceramic sample with few micrometer grain size and hundreds of volts to a thin film.

2.2 Temperature dependence of the grain boundary potential, Ψ_{gb}

In our earlier work[25] we demonstrated that within a relatively narrow range of temperatures the relation $n \cdot T = const$ is valid. Here we discuss this relation more in detail and outline its

applicability limits more thoroughly. To consider the temperature dependence of Ψ_{gb} in our model two important facts should be noted:

(a) If the Q_{gb} starts to dissipate, i.e., the depth of the potential trap holding the Q_{gb} becomes comparable to the thermal energy, k_BT, then prediction of the Ψ_{gb} and the I_{gb}-U_{gb} relationship requires precise knowledge of the temperature dependence of the Q_{gb}. Such consideration is however beyond the scope of the present study.

(b) As we mentioned in our earlier work[25], the depth of the traps at the grain boundary is largely comparable to the band gap of the material, which typically exceeds 3 eV in ionic conductors. It would suggest that even at 900 °C, k_BT is lower than the trap depth by a factor of 10 even if the trap depth is assumed to be only ~1 eV so that in ionic conductors the Q_{gb} is likely retained over a temperature spanning hundreds of degrees. Here we discuss the temperature dependence of the Ψ_{gb} for two practically important cases where: **(i)** the C_i^+ remains constant with temperature (e.g. oxygen-ion conductors) and **(ii)** where C_i^+ decreases with temperature (e.g. proton conductors).

As demonstrated earlier for the case of Gaussian-shape charge distribution of the Q_{gb} [25], the I_{gb}-U_{gb} characteristic is defined by two dimensionless parameters, *a* and *d*. It should be noted that even if the Q_{gb} remains constant and C_i^+ is independent of temperature, both *a* and *d* will still vary with temperature because L_D depends on temperature. However, it should also be noted that the ratio $a/d = Q_{gb} \cdot d_{real} / C_i^+$ remains constant. With the same mathematical approach and computational codes as in ref.[25], we have calculated $\varphi_{gb} = \Psi_{gb} / V_{th}$ for a number of different values of Q_{gb}, d_{real} and C_i^+ as a function of temperature. The results of the calculations show that in the relatively lower temperature range (T < 1000 K) and for $\varphi_{gb} > 5$, the φ_{gb} changes

$$\varphi_{gb} = B / T + 1, \quad (4)$$

where the parameter, *B*, with a dimension of characteristic "temperature", lies within the range of 1,300-20,000 K (Fig. 1) and depends on the Q_{gb}, d_{real}, and C_i^+ in a rather complex manner (Table 2). Note however that Eq. (4) is valid only for the temperatures low enough to provide $\varphi_{gb} >> 1$ and in fact $\varphi_{gb} \to 0$ as $T \to \infty$ (see 11 and 12 in Figure 2), implying that heating

eventually eliminates the potential barrier altogether. The dependence of φ_{gb} on temperature (Eq. (4)) within the relatively lower temperature region gives $\Psi_{gb}/V_{th} = \Psi_{gb}/(k_B T/q) = B/T + 1$ (Figure 2) and, therefore:

(5) $$\Psi_{gb} = Bk_B/q + V_{th}$$

Our model predicts that the power law behavior of the I_{gb}-U_{gb} relationship occurs only at $\varphi_{gb} > 5$ ($\Psi_{gb} > 5V_{th}$), i.e $Bk_B/q > 4V_{th}$ from Eq. (5). Hence Eq. (5) implies a very weak dependence of the Ψ_{gb} on temperature as long as the charge remains trapped. For $\varphi_{gb} > 5$, the relation $n = 0.41\ \varphi_{gb}$[25] and Eq. (5) results in $n = 0.41 \cdot (B/T + 1)$ or

(6) $$T(n - 0.41) = 0.41 \cdot B = const$$

which is independent on temperature for a given sample as long as the condition $\Psi_{gb} >> V_{th}$ is held true. Again the power law is only observable for $\varphi_{gb} > 5$, n is usually greater than 2, in most practical cases Eq. (5) can be simplified to $T \cdot n \approx const$.

2.3 Materials with strong dependence of C_i^+ on temperature

If C_i^+ rapidly changes (often increases) with temperature, e.g. immobile vacancies become mobile upon temperature rise or the case of electrons in semiconductor, then the influence of the blocking grain boundaries on the conductivity quickly diminishes. It is worth noting that in the Gaussian distribution Eq. (2) the parameter a is proportional to $1/\sqrt{C_i^+}$ while d is proportional to $\sqrt{C_i^+}$. Therefore, increase in C_i^+ decreases a and increases d. Both factors result in the decrease in φ_{gb}, leading to a decrease of the power value, n, of the I_{gb}-U_{gb} relationships followed by disappearance of the non-linear region altogether.

The situation may become considerably more complex if the C_i^+ decreases with temperature in a material, e.g. Y-doped $BaCeO_3$, a well-known proton conductor. The data for water uptake in this proton conductor presented in ref. [36], can be quite accurately reproduced by a mass action law (the Langmuir curve) with $\Delta H = +63\ \mathrm{kJ \cdot mol^{-1}}$ and $\Delta S = +76\ \mathrm{J \cdot mol^{-1}K^{-1}}$ (with an accuracy better than one percent). One mole of water uptake introduces two moles of protons in such proton conductors according to the water incorporation reaction given as:

(7) $$V_O^{\bullet\bullet}(s)+O_O^x(s)+H_2O(g)\leftrightarrow 2OH_O^{\bullet}(s),$$

using the Kroeger-Vink notation. We assume, for the example shown in Figure 3, that the total charge trapped at the grain boundary is $Q_{gb} = 1.8\cdot10^{-5}\ C/cm^2$. This is equivalent to the number of protons trapped by 20% of oxygen on (100) plane of $BaCeO_3$. Under this assumption, we have simulated φ_{gb} and deduced the power, n, as a function of temperature. We further assumed that the contribution of the oxygen vacancies to the conductivity is much smaller than that of protons because the former has much lower mobility at least at moderate temperatures. As clearly seen in Figure 3, as long as the changes in the C_i^+ are small, n decreases with temperature. However, at temperatures where water loss becomes considerable our model predicts that n will start rising. Indeed in a temperature span of less than 200K, water loss decreases C_i^+ by several orders of magnitude, where T changes barely by one third (Figure 3a). In view of the fact that $a \propto 1/\left(\sqrt{C_i^+}\cdot\sqrt{T}\right)$ and $d \propto \left(\sqrt{C_i^+}/\sqrt{T}\right)$, the influence of $\sqrt{C_i^+}$ is clearly dominant. Decrease of C_i^+ causes both increase in the effective charge, a, and decrease in the effective thickness of the grain boundary, d. Both factors lead to a rise in the Ψ_{gb} with temperature. Thus, an increase in the value of n upon heating is an indication of a decrease in C_i^+. Although some influence of the oxygen vacancies on the electrical properties may be inevitable and Figure 3 provides a qualitative description, nevertheless the conductivity still remains predominantly protonic in the temperature regions under consideration. Therefore, increase in the power, n, shown in Figure 3 as a result of decrease in proton concentration should be experimentally observable.

3 Experimental results and discussion

3.1 Determination of the I_{gb} - U_{gb} relationship of a polycrystalline ceramic

In general, a bicrystal containing a highly blocking grain boundary with reversible electrodes is considered to be an ideal sample to investigate I_{gb}-U_{gb} relationship. In such a sample U_{gb} can be approximated as the external dc-bias applied to the sample, U_{dc}, since the dc-resistance of the sample, R_{dc}, is predominantly determined by the resistance across the grain boundary, R_{gb} (i.e. $U_{gb} = U_{dc}R_{gb}/R_{dc} \approx U_{dc}$ since $R_{dc} = R_b + R_{gb} + R_{el} \approx R_{gb}$ where R_b and R_{el} being the resistance in the bulk and the overpotential at the electrodes, respectively). On the other hand,

chemically homogeneous bicrystals of ionic conductors are rarely available because of various technical difficulties in preparation associated with their high melting temperature. Therefore the I_{gb}-U_{gb} relationships to be discussed below were determined using polycrystalline samples with large grain size (typically > 20 μm). The condition of $R_{dc} \approx R_{gb}$ was still held true for all the samples investigated as confirmed by e.g. Figure 3, which displays a representative impedance spectrum (viz a Nyquist plot) of 1 mol% Sm-doped CeO_2 (SDC) measured at 450 ˚C under different U_{gb}. The semicircles corresponding to the bulk (the inset) and the electrode (not noticeable) are negligibly small compared to the one for the grain boundary (the main panel). Therefore it can be approximated that $U_{gb} \approx U_{dc} / N_{gb}$ where N_{gb} is the number of grain boundaries in the polycrystalline samples which can be estimated based on the BLM, and $I_{gb} \approx U_{gb} / R_{gb}$ accordingly.

3.2 The I_{gb}-U_{gb} characteristics of the grain boundaries and the temperature dependence of the Ψ_{gb}

3.2.1 Oxygen-ion conductors

As clearly seen in Figure 4, the grain-boundary impedance in SDC measured in dry air systematically reduces with U_{dc}, while the bulk impedance remains unchanged, demonstrating that the requirements for reliable measurements of dc-bias dependence of the grain-boundary impedance using EIS discussed in the previous section is met. The resulting I_{gb}-U_{gb} relationships at different temperatures are shown in Figure 1. It is obvious that; (i) the I_{gb}-U_{gb} relationships follow the power law ($I_{gb} \propto U_{gb}^{n}$), displaying two linear regions on the log-log plot which appear at the U_{gb} below ~$2V_{th}$ and above ~3-4V_{th}, respectively. The value of the power n in the first linear region at the lower U_{gb} is almost exactly 1, independent of temperature measured, indicating that the grain boundary serves as a simple resistor in this region: (ii) Furthermore such an ohmic relationship continues until a relatively high bias of ~$2V_{th}$. (iii) In the second linear region at the higher U_{gb}, on the other hand, the value of n systematically decreases from 2.69 to 2.22 as temperature increases from 648 to 723 K to show $n \cdot T \approx const$. These observations are precisely what our model predicts whilst the TE model fails to reproduce the I_{gb}-U_{gb} characteristics observed. Similar I_{gb}-U_{gb} characteristics were also observed for ceria

doped with La^{3+} and Gd^{3+} (the plots are not shown). All these results together with those previously reported for YDC thus confirm that our model is reliably reproduce the I_{gb}-U_{gb} characteristics in oxygen-ion conductors and is indeed very robust.

Figure 5 shows the Ψ_{gb} in the ceria doped with La^{3+}, Sm^{3+}, and Gd^{3+} as a function of temperature, determined using the relation $n \cdot T = (0.41q/k_B)\Psi_{gb}$. Also included for comparison is the Ψ_{gb} in YDC previously reported[25]. As can be seen, the values of the Ψ_{gb} are reasonably constant in the temperature region of interest regardless of the dopant. It should be noted that the Ψ_{gb} decreases with the dopant size (Gd < Sm < La), consistent with the fact that the R_{gb} in these lanthanides-doped ceria decreases with the dopant size (i.e. I_{gb} increases with the size of the dopant).

3.2.2 Proton conductors

Unlike the oxygen-ion conductors, the C_i^+ may not remain constant with temperature in proton conductors, and starts to decrease typically at around 600 K in those with perovskite structure in particular as previously mentioned. Our model predicts in such a case that the relation $n \cdot T \approx const$ is no longer valid and the Ψ_{gb} should increase with temperature (Section 2.3 above). To verify our simulation results, we measured the I_{gb}-U_{gb} characteristics of a proton conductor, 2 mole% Y-doped $BaZrO_3$ (BZY2). Doped $BaZrO_3$ is one of the most intensively studied proton conductors as a solid electrolyte for fuel cell applications because of their superior chemical stability and high protonic conductivity in the bulk at relatively low temperatures.[36] They are also known for their high grain-boundary resistance attributed to substantial depletion of protons in the space-charge zones, leading to formation of a Ψ_{gb} similar to what is observed for doped ceria.[11-13,15-19,36]

Figure 6 shows a representative Nyquist plot of BZY2 and the resulting I_{gb}-U_{gb} relationships we measured at different temperatures. The similar I_{gb}-U_{gb} characteristics to those observed earlier for the ceria samples discussed above can also be found for the proton conductor: Up to U_{gb} of ~$2V_{th}$, the relationship is ohmic (n = 1) regardless of temperature measured and the

second linear region with n > 1 appear at the U_{gb} above ~ $5V_{th}$. The second linear region may not be fully seen in

Figure 6. The grain size (~3 μm) of this sample is relatively large compared with that of most BZY ceramics previously reported and yet much smaller than those of the ceria samples discussed above. Therefore to measure the complete linear behavior at higher U_{gb}, it was necessary to apply even higher dc-bias than +30V which is the maximum bias we could apply to the sample with the analyzer used. Nevertheless it is still obvious that the I_{gb}-U_{gb} relationship in the proton conductor obeys the power law. In fact, the power law behavior of the I_{gb}-U_{gb} relationship for some proton conductors were reported previously.[12,13,15,37] The Ψ_{gb} in BZY2 estimated from the relation, $nT = (0.41q/k_B)\Psi_{gb}$ is shown in Figure 7 as a function of temperature. Indeed the value increases from 2.24 to 2.47 as temperature increases from 573 to 723 K, leading to increase in Ψ_{gb} with temperature, consistent with our model prediction.

3.3 Comparison between the linear diffusion and thermionic emission (TE) models.

It is of interest to compare our linear diffusion model with the TE model. In the TE model a grain boundary is often treated as either an infinitely thin potential barrier or a thermodynamically well-defined secondary phase with an appreciable thickness. Accordingly, when the TE model is applied to interpret the I_{gb}-U_{gb} relationships experimentally measured for ionic conductors, it immediately assumes that a grain boundary in an ionic conductor is considered either the former or the latter and the current across the Ψ_{gb} at the grain boundary is attributed to thermionic emission of ions over such a barrier. However, in our view, such an assumption is rather inappropriate because: a) a grain boundary hinders ionic diffusion primarily due to the presence of an electric field with a spatial profile and, therefore, cannot be treated as an infinitely thin barrier; b) thermionic emission between two identical grains does not represent an adequate picture of ionic transport across the grain boundary because both grains have the same chemical potential of the ions. Therefore it is necessary to assume a grain-boundary core to be a secondary phase with distinctively different thermodynamics from the grains. In light of the fact that the grain-boundary core is in most ion-conducting ceramics is rather a thin layer with a thickness of about 1-2 unit cells, it is rather difficult to justify the assumption.

There is also considerable difficulty in practical interpretation of a given I_{gb}-U_{gb} curve with the equation derived based on the TE model.

(i) According to the TE model, once the U_{gb} becomes a fraction of V_{th} the I_{gb}-U_{gb} curve should deviate from the ohmic behavior to eventually show an exponential relationship as mentioned earlier. However, an exact form of the I_{gb}-U_{gb} relationship cannot be predicted. Examination of the I_{gb}-U_{gb} curves for ionic and proton conductors consistently indicates that the current is linearly proportional to U_{gb} well above V_{th} (see Figure 1 and

Figure 6), which, however, perfectly agrees with the prediction based on our linear diffusion model [25].

(ii) At sufficiently high voltages, $U_{gb} > V_{th}$, the TE model predicts that the I_{gb}-U_{gb} relationship can be simplified because the depletion layer for the current under "forward bias" is nearly vanished ("a flat band" state using a semiconductor terminology): The current across a grain boundary is described by [26-28]:

$$j = j_0 \cdot \exp\left(\frac{U_{gb1}}{V_{th}}\right) \cdot \left(1 - \exp\left(-\frac{U_{gb}}{V_{th}}\right)\right) \tag{8}$$

where j_0 is the equivalent of "exchange current", which is a product of the Richardson constant and a factor taking into account the Ψ_{gb}. U_{gb1} is a fraction of U_{gb} that drops on the remaining depletion layer. Although it does not allow a direct estimate, the limiting cases for it are very clear. For a very small U_{gb}, the back-to-back depletion layers should equally share the U_{gb} and thus $U_{gb1} \approx U_{gb}/2$ can be assumed. However, once one of the depletion layers nearly vanishes, i.e., $U_{gb} >> V_{th}$, $U_{gb1} \approx U_{gb}$ must be held true and the Eq. (8) simplifies to

$$j = j_0 \cdot \exp\left(\frac{U_{gb}}{V_{th}}\right) \tag{9}$$

The relationship between $\ln(j/j_0)$ and U_{gb} should then be close to be linear and the slope $d\ln(j/j_0)/dU_{gb}$ is expected to be strictly $1/V_{th}$. However the I_{gb}-U_{gb} relationships experimentally measured for the ionic and the protonic conductor, if fitted to (9), leads to the slopes which are much lower than $1/V_{th}$: about $0.5/V_{th}$ for doped ceria and $0.3/V_{th}$ for BZY2 we

investigated. These facts contradict the expectations because it would imply that even at $U_{gb} > 8$ V_{th}, none of the depletion layers is really compensated. Moreover, for the proton conductor it would imply that most of the voltage falls on the depletion layer for the current under the "forward bias", which is rather impossible. On the other hand, our linear diffusion model explains the I_{gb}-U_{gb} relationships of the ionic conductors of interest without invoking and further assumptions.

3.4 The Ψ_{gb} determined by the conventional Schottky-type barrier model

Figure 5 includes the values of the Ψ_{gb} in doped CeO_2 determined by the ratio of the specific grain-boundary resistivity, ρ_{gb}, to the bulk counterpart, ρ_{gb}, the conventional method based on the BLM, given as[29]:

$$r = \frac{\rho_{gb}}{\rho_b} = \frac{\exp[q \cdot \Psi_{gb}/(k_B T)]}{2 \cdot q \cdot \Psi_{gb}/(k_B T)} \quad (10)$$

As clearly seen, the values (~0.45-0.55V depending upon the dopant) are noticeably higher than the corresponding Ψ_{gb} (~0.35-0.40 V) determined from the I_{gb}-U_{gb} model. It is also interesting to note the values constantly increase even within such a relatively narrow range of the temperature regardless of the dopant, while those determined from our I_{gb}-U_{gb} model remain nearly constant as discussed earlier. Moreover, the Ψ_{gb} determined using Eq. (10) shows no relationship with the dopant size (i.e. $\Psi_{gb}(La) \le \Psi_{gb}(Gd) < \Psi_{gb}(Sm)$), while the Ψ_{gb} determined from the I_{gb}-U_{gb} model decreases with the dopant size (i.e. $\Psi_{gb}(La) \le \Psi_{gb}(Sm) < \Psi_{gb}(Gd)$).

The discrepancy between the Ψ_{gb} determined using the two different models becomes even greater for the proton conductor (Figure 7). The Ψ_{gb} in BZY2 determined using Eq. (10) is nearly 1V, while the value (~0.35V) from our model is similar to those observed for doped CeO_2. Apparently, such an unusually high value of the Ψ_{gb} in BZY2 resulted from Eq. (9) is due to the very high value of ρ_{gb}/ρ_b consistently reported for BZY. It is worth noting however that Eq. (10) is justified upon two conditions: **a)** The space charge trapped at the grain boundary is concentrated in a very narrow region; **b)** the space charge is the sole reason for the obstruction of the current flow at the grain boundary. The assumption (a) that the charge at grain boundaries is

confined in a very narrow region (i.e. the order of magnitude of a Debye length) may not be universal, though often correct, and one can offer a very simple case against this assumption. The resistance of the space charge region (the one inferred from impedance spectra) is a product of its average resistivity and thickness. If the charge trapped at the grain boundaries has low density but distributed over a region which is substantially wider than Debye length, the degree of depletion and the Ψ_{gb} can be low. Nonetheless, the resistance of the depleted region at the grain boundary can still be very high because of its sheer thickness. It may be expected that wide distribution of the trapped charges should result in a corresponding increase in the capacitance of the grain boundaries. However, the change may not be easily detectable because of the uncertainty in the grain boundary capacitance experimentally determined due to the uncertainty in the grain size estimated. Furthermore, a small change in the thickness of the region where charges are trapped, a, results in a large change in the Ψ_{gb}.

The validity of the approximation (a) may also be challenged by the following considerations. Electric field at a grain boundary with a Ψ_{gb} close to 1 V and Debye length of ~ 1 nm, would exceed 10 million V/cm, corresponding to electrostatic energy of ~10 $\mathrm{kJ \cdot mol^{-1}}$ and should lead to a lattice distortions of at least 1% even with the most modest estimate of the electrostriction effect. Moreover, in such an enormous electric field, ion hopping between two neighboring sites in the lattice separated by ~0.2 nm would gain an energy of 0.2 eV, which is more than 1 k_BT and well comparable to the activation energy of the ion diffusion (typically 0.5-1 eV in such ionic conductors). In view of the complexity of the problem, we will provide a more detailed comparison of the grain boundary assessment by both approaches in a forthcoming work.

b) Even in the cases where the obstruction of ion transfer at the grain boundaries is not due to space charge (but e.g. second phase and/or large structural distortions), the Nyquist plot will still show a semicircle corresponding to the resistance and capacitance of grain boundaries. In such a case, the grain boundary impedance cannot be interpreted in terms of the depletion layers and space charge. It is important to be noted, though, that the linear diffusion model extracts the Ψ_{gb} from the dependence, $d(\ln(I))/d(\ln(V))$, rather than taking an absolute values. Consequently, presence of an "extra resistance" irrelevant to space charge has little influence on our model compared to the calculations based on the grain-boundary resistivity. A priori, one

cannot say which of these arguments is at work, however, both theories have their limitations. We will provide a detailed comparison of both theories in the forthcoming work.

4 Conclusions

We have demonstrated that the linear diffusion model we proposed accurately reproduces the I_{gb}-U_{gb} relationships of various oxygen-ion and proton conductors such as rare earth-doped ceria and BZY2, respectively. For the case of doped ceria, the model provides explanations for the "power law" behavior of the I_{gb}-U_{gb} relationships and also for the consistent change in the Ψ_{gb} with the ions radii. The model correctly predicts the very weak dependence of the Ψ_{gb} on temperature in doped ceria experimentally observed and allows for determination of the value of the Ψ_{gb} from the power, n, experimentally measured. Furthermore the model also provides a plausible explanation for the increase in the Ψ_{gb} with temperature in BZY2, which is attributed to the decrease in the number of protons in the bulk as temperature increases. Combining these results together, we conclude that the linear diffusion model we proposed is very robust and thus applicable to grain boundaries in a large variety of ionic conductors of practical interest.

5 Experimental methods

The rare-earth-doped ceria powders were synthesized by a co-precipitation method using ammonium carbonate as the precipitating agent and nitrates for precursors. The synthesized powders were calcined at 700°C for 2 hours. The pure cubic phases of the calcined powders were confirmed by XRD patterns (Scintag X-ray Diffractometer). For EIS characterizations, the powders were formed into cylindrical pellets, and pressed with 300 MPa using a cold isostatic press, followed by sintering at 1600°C for 10 hours under ambient air. The densities of the sintered pellets determined using the Archimedes method were higher than 98% of the theoretical density. The grain size of the samples estimated from the microstructure images taken using a scanning electron microscope (FE-SEM S-4100T, Hitachi) were typically larger than 20 μm. Prior to the microstructure imaging, the samples were mechanically polished and thermally etched at 1300°C for 1 hour. The diameter and thickness of the final pellets are typically ~ 6.3 and 0.5-1.0 mm, respectively. BZY2 powder was synthesized via solid-state reaction as described in ref.[38] and pressed cold isostatically at 220 MPa followed by sintering at 1800°C for

30 hours in air. The relative density was ~ 97% and the grain size was 3.3 microns. The final sample dimension was ~1.3×2.2×0.2 mm. Pt/Ag electrodes were applied on both sides of the samples prior to electrical measurements.

EIS measurements on the samples were carried out using a Novocontrol alpha analyzer (Novocontrol-AN) as a function of external dc-bias and temperature. The fittings of the measured impedance spectra were performed using Z-View. The representative bulk and the grain-boundary resistances and capacitances resulting from the best fit for ceria and BZY2 samples are the following: For SDC, R_b and R_{gb} at 400°C are ~1.4×10^3 and 5.2×10^6 Ω, respectively. In the case of BZY2, R_b and R_{gb} are ~5.5×10^2 and 1.8×10^6 Ω, respectively, at the same temperature. C_b and C_{gb} at 400°C for the former are 8.6×10^{12} and 2.2×10^8 F, respectively, and 2.6×10^{11} and 6.5×10^5 F for the latter.

6 Acknowledgements

S.K. and I.L. wish to thank the US-Israel Binational Science Foundation and Minerva foundation for funding this research. I.L. wishes to acknowledge the Nancy and Stephen Grand Research Center for Sensors and Security. The research is also made possible in part by the generosity of the Harold Perlman Family.

7 Figures and tables

Table 1. Normalization units to the dimensionless equation of ionic transport

(a) distance: $x = X / L_D$, where $L_D = \sqrt{\frac{\varepsilon \cdot \varepsilon_0 \cdot k_B \cdot T}{q^2 \cdot C_i^+}}$ is Debye length; ε is a dielectric constant, ε_0 is the dielectric permittivity of vacuum

(b) potential: $\varphi = \Psi / V_{th}$, where $V_{th} = k_B \cdot T / q$ is thermal voltage

(c) electric field: $\phi = -\frac{E}{E_0} = -\frac{d\varphi}{dx}$, where $E_0 = V_{th} / L_D$

(d) concentration: $n^+(x) = C_i^+(X) / C_i^+$,

(e) current: $j = J / J_0$ where $J_0 = C_i^+ \cdot D \cdot q / L_D$, where D is the ion diffusivity

Table 2 Values used for calculation of the temperature dependence of the grain-boundary potential Figure 2

Set #in Figure 2	Q_{gb} , $10^{-5}\ C/cm^2$ (Eqs. (**2**) and (**3**))	d_{real} , nm	$q \cdot C_i^+$ $10^{20}\ C/cm^3$	Slope, K (±0.5%)
1	4.57	1	3.22	16493
2	1.83	1	0.805	11868
3	3.66	1	3.22	9666
4	4.57	0.25	0.805	7439
5	1.83	1	1.61	4827
6	2.74	1	3.22	4571
7	1.83	0.25	3.22	2981
8	1.83	0.5	3.22	2403
9	0.914	0.25	1.61	1500
10	1.83	1	3.22	1295
11	0.914	0.5	3.22	Not applicable
12	0.914	1	3.22	Not applicable

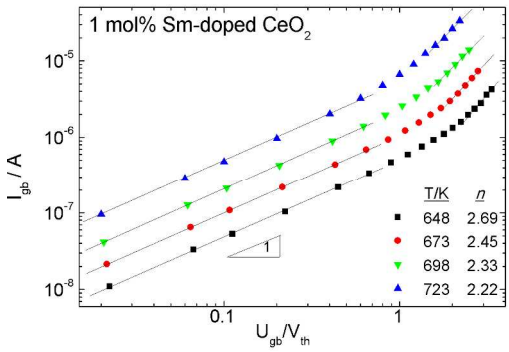

Figure 1. Current voltage characteristics of the grain boundaries in 1mol% doped Sm-doped ceria

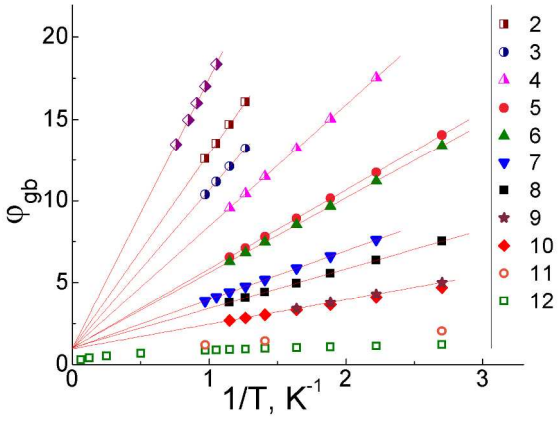

Figure 2. (a) Dependence of φ_{gb} on temperature for various values of Q_{gb} , d_{real} and C_i^+ (see Table 2)

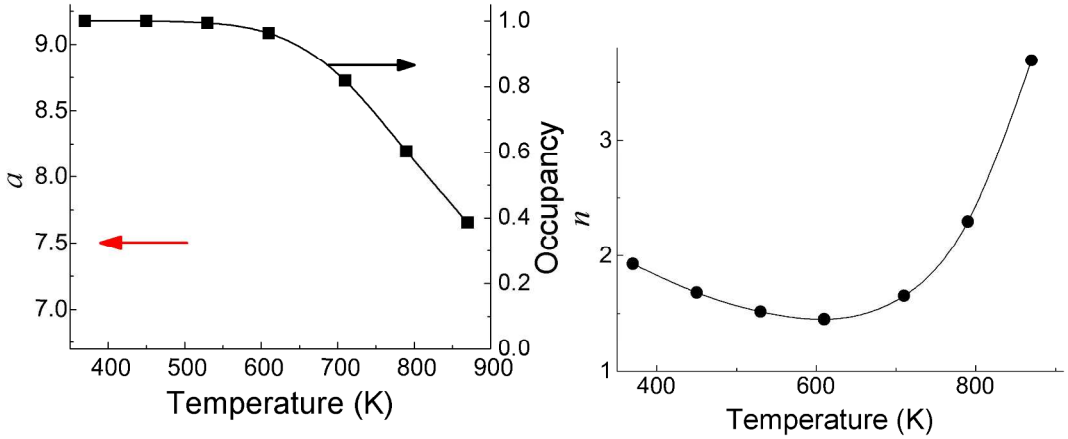

a) b)

Figure 3. **(a)** The dependence of the occupancy of the vacancies by protons (from Ref.[36]) and the corresponding effective trapped charge at the grain boundary, a (see Eq. (2)) as a function of on

temperature; **(b)** Changes in power n as a function of temperature predicted by the linear diffusion model.

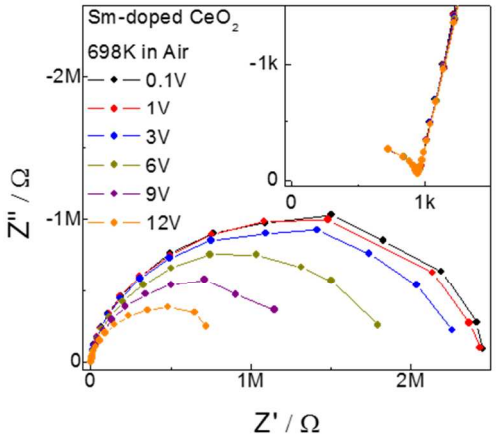

Figure 4. A representative impedance spectrum (viz a Nyquist plot) of 1 mol% Sm-doped CeO_2 (SDC) measured at 425˚C under different U_{gb}

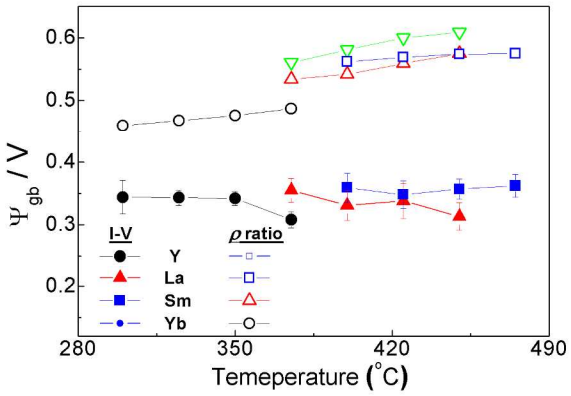

Figure 5 Grain-boundary potential for rare earth doped ceria calculated from the linear diffusion model (full symbols) and from the resistivity ratio (hollow symbols).

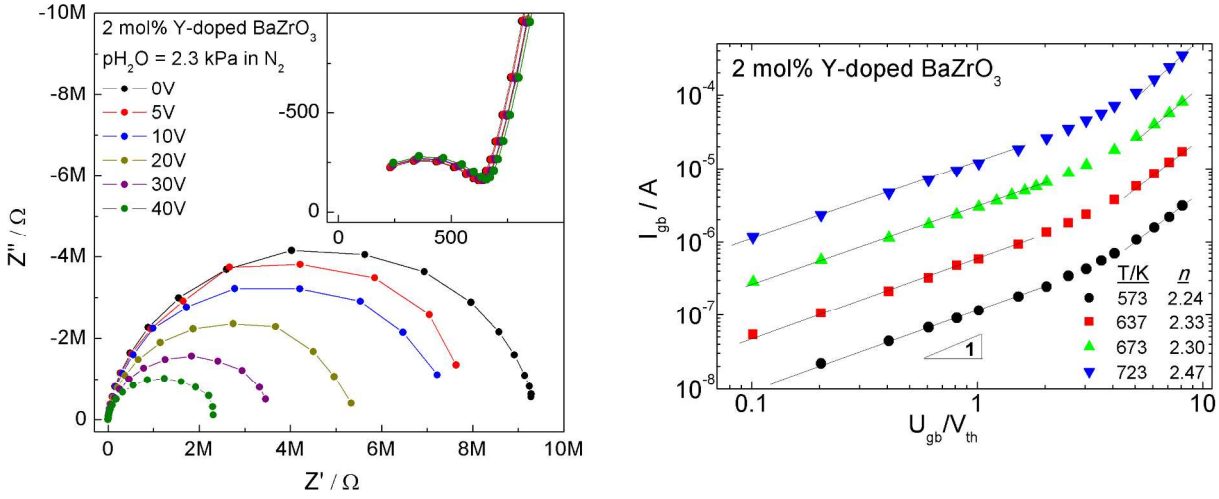

Figure 6. A representative Nyquist plot of 2 mol% Y-doped $BaZrO_3$ (BZY2) measured at 350˚C under different U_{gb} (left) and the current voltage characteristics of the grain boundaries in 2 mol% doped Y-doped barium zirconate (right).

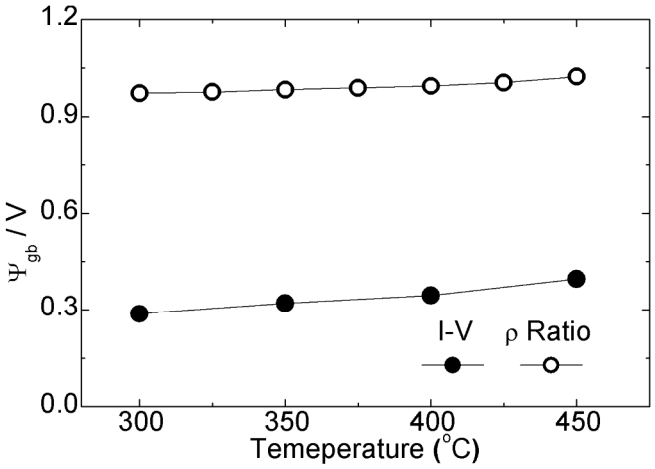

Figure 7 Grain-boundary potential, Ψ_{gb}, of BZY2 calculated from the linear diffusion model (I-V - full symbols) [25] and by the resistivity ratio (ρ - Ratio - hollow symbols).

8 References

1 J. B. Goodenough, *Ann Rev Mater Res* 2003**,** ***33***, 91-128.
2 J. B. Goodenough and Y. Kim, *Chem Mater* 2010**,** ***22***, 587-603.
3 S. Kim and J. Maier, *J. Elecrochem. Soc.* 2002**,** ***149***, J73-J83.
4 S. Kim, J. Fleig, and J. Maier, *Phys Chem Chem Phys* 2003**,** ***5***, 2268-2273.
5 H. J. Avila-Paredes and S. Kim, *Sol. State Ionics* 2006**,** ***177***, 3075-3080.
6 J. S. Lee, U. Anselmi-Tamburini, Z. A. Munir, and S. Kim, *Electrochem. Solid-State Lett.* 2006**,** ***9***, J34-J36.
7 H. J. Park and S. Kim, *J Phys Chem C* 2007**,** ***111***, 14903-14910.
8 R. A. De Souza, M. J. Pietrowski, U. Anselmi-Tamburini, S. Kim, Z. A. Munir, and M. Martin, *Phys Chem Chem Phys* 2008**,** ***10***, 2067-2072.
9 H. J. Park and S. Kim, *Sol. State Ionics* 2008**,** ***179***, 1329-1332.
10 H. J. Avila-Paredes, K. Choi, C. T. Chen, and S. Kim, *J Mater Chem* 2009**,** ***19***, 4837-4842.
11 C. T. Chen, C. E. Danel, and S. Kim, *J Mater Chem* 2011**,** ***21***, 5435-5442.
12 F. Iguchi, C. T. Chen, H. Yugami, and S. Kim, *J Mater Chem* 2011**,** ***21***, 16517-16523.
13 C. T. Chen, K. Choi, and S. Kim, *Phys Chem Chem Phys* 2012**,** ***14***, 9047-9049.
14 X. Guo and R. Waser, *Prog Mater Sci* 2006**,** ***51***, 151-210.
15 M. Shirpour, R. Merkle, C. T. Lin, and J. Maier, *Phys Chem Chem Phys* 2012**,** ***14***, 730-740.
16 M. Shirpour, R. Merkle, and J. Maier, *Sol. State Ionics* 2012**,** ***225***, 304-307.
17 M. Shirpour, R. Merkle, and J. Maier, *Sol. State Ionics* 2012**,** ***216***, 1-5.
18 M. Shirpour, B. Rahmati, W. Sigle, P. A. van Aken, R. Merkle, and J. Maier, *J Phys Chem C* 2012**,** ***116***, 2453-2461.
19 C. Kjolseth, H. Fjeld, O. Prytz, P. I. Dahl, C. Estournes, R. Haugsrud, and T. Norby, *Sol. State Ionics* 2010**,** ***181***, 268-275.
20 A. Tschope, *Sol. State Ionics* 2001**,** ***139***, 267-280.
21 A. Tschope, E. Sommer, and R. Birringer, *Sol. State Ionics* 2001**,** ***139***, 255-265.
22 M. G. Spencer, W. J. Schaff, and D. K. Wagner, *J. Appl. Phys.* 1983**,** ***54***, 1429-1440.
23 S. S. Simeonov, *Phys. Rev. B* 1987**,** ***36***, 9171-9181.
24 G. E. Pike, *Phys. Rev. B* 1984**,** ***30***, 795-802.
25 S. K. Kim, S. Khodorov, C. T. Chen, S. Kim, and I. Lubomirsky, *Phys Chem Chem Phys* 2013**,** ***15***, 8716-8721.
26 G. E. Pike and C. H. Seager, *J. Appl. Phys.* 1979**,** ***50***, 3414-3422.
27 G. GreuterBlatter and F. Greuter, *Phys. Rev. B* 1986**,** ***33***, 3952-3966.
28 R. Stratton, *P Phys Soc Lond B* 1956**,** ***69***, 513-527.
29 J. Fleig, S. Rodewald, and J. Maier, *J. Appl. Phys.* 2000**,** ***87***, 2372-2381.
30 Y. Gil, O. M. Umurhan, Y. Tsur, and I. Riess, *Sol. State Ionics* 2008**,** ***179***, 1187-1193.
31 A. Leshem, E. Gonen, and I. Riess, *Nanotechnology* 2011**,** ***22***.
32 I. Riess, *Z. Phys. Chem.* 2005**,** ***219***, 1-22.
33 I. Riess, *J. Electroceram.* 2006**,** ***17***, 247-253.
34 I. Lyubomirsky, V. Lyahovitskaya, and D. Cahen, *Appl. Phys. Lett.* 1997**,** ***70***, 613-615.
35 D. Kalaev and I. Riess, *Sol. State Ionics* 2012**,** ***212*** 26.
36 K. D. Kreuer, *Ann Rev Mater Res* 2003**,** ***33***, 333-359.
37 C. T. Chen, S. K. Kim, M. Ibbotson, A. Yeung, and S. Kim, *Int J Hydrogen Energ* 2012**,** ***37***, 12432-12437.
38 F. Iguchi, N. Sata, T. Tsurui, and H. Yugami, *Sol. State Ionics* 2007**,** ***178***, 691-695.